

ORBIT MEASUREMENT AND CORRECTION IN THE LNLS SYNCHROTRON LIGHT SOURCE

R.H.A. Farias, L.C. Jahnelt, Liu Lin, D. Macedo, F.S. Rafael, A.R.D. Rodrigues and P.F. Tavares

Laboratório Nacional de Luz Síncrotron - LNLS/CNPq
Caixa Postal 6192 - 13081-970 Campinas - SP - Brazil.

Abstract

The orbit measurement and correction system of the LNLS synchrotron light source is presented. Measurements of the correction matrix, orbit stability and reproducibility are presented and discussed.

1 INTRODUCTION

The LNLS Synchrotron Light Source consists of the 1.37 GeV electron storage ring UVX and a 120 MeV injector LINAC. Commissioning of the ring started in May 1996 and users have had access to the machine since November 1996. It became clear from the early stages of beam line commissioning that orbit reproducibility from fill to fill as well as orbit stability over long periods (several hours) are critical performance figures of the light source from the user's point of view. In this report, we describe the main parts of the correction system, including the BPM's and their calibration procedures, the control system facilities for orbit measurement and manipulation and present results of measurements of orbit stability and reproducibility.

2 HARDWARE

The UVX storage ring has 24 beam position monitors (striplines) distributed along its six superperiods. The stripline signals are read by 6 commercial electronic readout modules (manufactured by BERGOZ, France). Since there is only one read-out module per superperiod, each module must read four different BPM's. This is accomplished by multiplexing those signals via a computer controlled RF switch-board, which allows the four monitors to be read in any order set by the high level control system. The total time for a complete scan of all four BPMS in a superperiod is dominated by the time needed by the RF switches to stabilise their output signal and it is 400 ms.

The BPM's were calibrated in a characterisation bench with a stretched wire to simulate the beam. A 476 MHz signal was applied to the stretched wire and the signals induced in the stripline were measured with a spectrum analyser. The bench was computer controlled so that the wire could be moved automatically in order to obtain a two dimensional map of the response of the striplines to the excitation by the wire. The resulting data were used to derive an offset of the electrical centre of the monitors

with respect to the geometrical centre and a gain factor. The offset and gain for each BPM characterise the geometry of the BPM as far as the linear response to beam position is concerned.

An off-set and gain were also determined for the BPM electronics (in fact, this offset and gain includes the effects not only of the electronics, but also of the cables, RF switches and connectors). The offset was determined with a calibrated four-way splitter fed by a 476 MHz signal and connected to the same cables, RF switches, connectors that take signals from the BPM's to their electronics (this measurement takes place in the machine). The measured dc voltages (horizontal and vertical) at the output of the BPM electronics give directly the off-set. The gain was determined by adding attenuators to two of the output ports of the four-way splitter and again measuring the voltages delivered by the BPM electronics. The calibration parameters for each BPM (geometrical) as well as those of the BPM electronics were organised in databases for the control system allowing the conversion of the voltages read by the control system to beam position in mm.

The BPM absolute accuracy is determined by the alignment procedure and is better than 0.2 mm. The BPM resolution is determined by the electronic noise and by the resolution of the AD converters used to read the BPM output voltages. The noise level in the electronics has been measured prior to installation with an RF generator substituting the beam and, without any averaging, was found to be $\pm 4 \mu\text{m}$ (at an equivalent beam intensity of about 5 mA). The resolution of the AD converters is $\pm 8 \mu\text{m}$. The overall resolution can be reduced to $\pm 2 \mu\text{m}$ by averaging the signal over 10 seconds.

The orbit correctors are 10 cm long C-type (vertical) and H-type (horizontal) magnets. There are 11 vertical and 18 horizontal correctors. They are capable of producing up to 70 gauss.m of integrated field, corresponding to 1.5 mrad deflection at 1.37 GeV.

3 SOFTWARE

It is possible to observe and store orbits as well as to perform simple arithmetic with stored orbits and newly acquired data. The acquisition cycle is fast enough that on-line observation of the orbits is possible and has proved useful in commissioning the energy ramp.

Orbit correction can be performed via three different methods: matrix, best correctors and harmonic. In all

methods, specific corrector and monitors can be excluded from the correction procedure by pointing and clicking, e.g., in order to eliminate known erroneous data. The proposed corrections may be examined before implementation in the machine and it is possible to implement a fraction of the correction. All calculations are performed in a remote Unix workstation where a model of the machine optics may be established either from the quadrupole and sextupole strengths as implemented in the machine (and derived from the measured excitation curves of the storage ring magnets) or by fitting the quadrupole strengths to the measured machine tunes. Both models are found to work equally well at the operating energy (1.37 GeV), but at injection energy it is mandatory to use the fitted model to get efficient correction. This is due to remnant field effects which make the quadrupole calibration curves less reliable at low energies as well as the spread between calibration curves of different quadrupoles connected to the same power supply larger.

During commissioning (and even in some user shifts) we often had the need to produce localised orbit bumps, eg. in order to look for vacuum chamber obstructions or produce special conditions for a beam line with minimal disturbance to the others. This can be accomplished easily once an optical model has been generated for the machine via a point and click interface.

4 MEASUREMENT RESULTS

4.1 Correction Matrix

In various correction methods one needs to know the *correction matrix* that relates changes in corrector strengths to changes in beam position within linear approximation. Figure 1 shows a comparison between calculated (from a fitted model of the machine optics) and measured correction matrix elements for two different horizontal correctors. The calculation is performed according to the well-known formula

$$x(s) = \frac{\sqrt{\beta(s)\beta(0)}}{2 \sin(\pi\nu)} \cos(\varphi(s) - \varphi(0) - \pi\nu) \quad (1)$$

One of the correctors (ACH04) is located in a dispersive straight section while the other (ACH01A) is located in a non-dispersive straight section. The discrepancies between theory and experiment may be ascribed partly to non-linearities in BPM response (for the larger orbit deviations, such as in BPM's AMP07A and AMP07B for corrector ACH01A) and partly to the fact that orbit perturbations produce energy changes which result in the addition of a periodic perturbation to the closed orbit proportional to the dispersion function and to the magnitude of the energy change. This can be more easily seen in the implementation of horizontal localized bumps and will be discussed further below. Note however in figure 2 that the difference between theory and

experiment closely resembles the machine dispersion function (being non-zero in even, i.e., dispersive sections) for corrector ACH04, except in section 9 where the orbit distortion is largest and the non-linearity effects are correspondingly more important. The inclusion of the energy change correction to the correction matrix elements was found to be essential to correct the horizontal orbit when the average uncorrected orbit is different from zero. Although this can in principle be dealt with by changing the RF frequency, in the particular case of the LNLS machine there is an appreciable change of the dipole magnets effective length as the energy is ramped, and the ability to correct orbits with non-zero average is needed in order to avoid changing the RF frequency during the ramp.

4.2 Orbit correction and reproducibility

We have found it necessary to apply the correction procedure iteratively (often beginning with a few iterations of the best correctors method and then turning to the matrix method as the orbit distortion gets smaller). The horizontal rms orbit deviation is reduced from 2 to 0.3 mm whereas the vertical rms orbit deviation is reduced from 2 to 0.4 mm (Figure 3).

More important than the orbit itself however, is the ability to reobtain the same orbit after each injection and energy ramping cycle. Figure 4 shows that simply ramping to a previously corrected configuration reproduces the orbit to within about 0.8 mm. We have therefore adopted the strategy of correcting the orbit towards a *standard* orbit previously considered as the best possible orbit we can get and with respect to which users align their beam lines. We have found (Figure 4) that we can reobtain this same orbit to within $\pm 60 \mu\text{m}$ at every injection by recorrecting the orbit before delivering the beam to users.

4.3 Orbit stability

The stability of the orbit has been analysed in two different temporal regimes: fast (few second) orbit fluctuations and long term (several hours) orbit drifts. Fast fluctuations are compatible with the BPM resolution.

Long term drifts (particularly of the vertical orbit) have been correlated to drifts in magnet temperatures, which has led us to include a temperature stabilisation system for the cooling water of the main ring magnets. Although this has decreased the orbit drift, we have found it necessary to implement an automatic orbit correction system that periodically (every few minutes) recorrects the orbit. With this system on, the vertical orbit is kept to within $\pm 30 \mu\text{m}$ of the initial orbit over 3-4 hours of a user run. Figure 5 shows the time evolution of the orbit envelope (maximum absolute orbit deviation along the machine) with the correction system on and off.

4.4 Orbit Manipulation

Figure 6 shows a measured localized horizontal bump as well as the calculated bump. The presence of *anti-bumps* in the dispersive sections of the lattice is a result of the change in energy of the beam due to the orbit distortion, as can be seen from the calculations that include this longitudinal-transverse coupling effect as well as the conventional orbit distortion formula above (Eq. 1).

5 CONCLUSIONS

The orbit measurement and correction system of the LNS UVX electron storage ring has proved to be versatile during commissioning and up to specifications for user runs. Orbit reproducibility from fill to fill is better than $60 \mu\text{m}$, long term orbit drifts can be kept below $\pm 30 \mu\text{m}$ by means of an automatic periodic correction. The effect of energy changes due to corrector kicks can be clearly seen in the correction matrix as well as in orbit bumps.

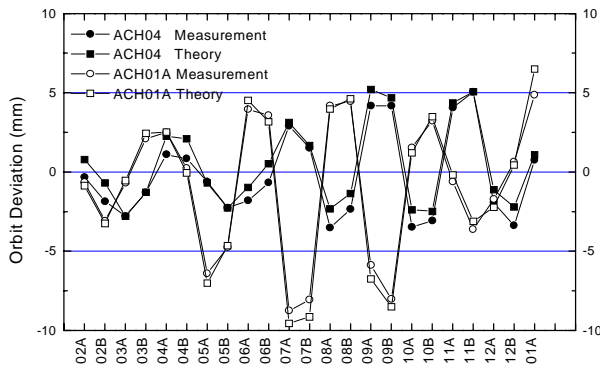


Figure 1: Calculated and measured orbit distortions for correctors located in non-dispersive (ACH01A) and dispersive (ACH04) straight sections.

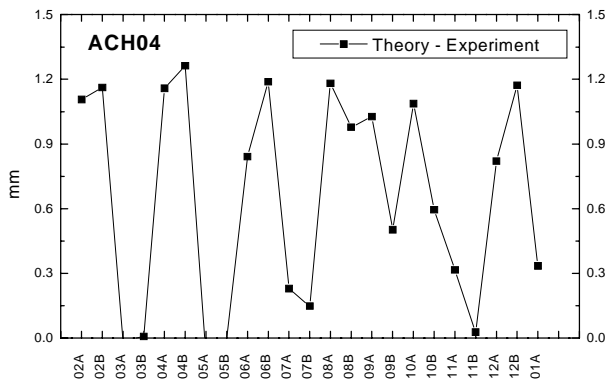


Figure 2: Difference between theoretical prediction and measurement for the orbit distortion produced by corrector magnet ACH04.

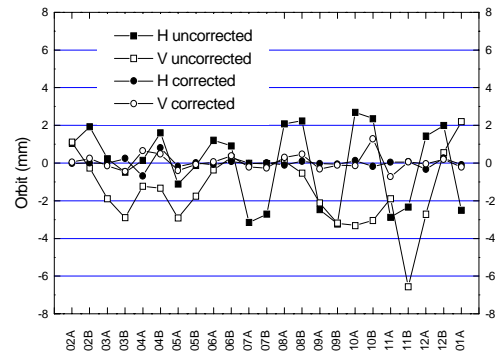


Figure 3: Uncorrected and corrected orbits at 1.37 GeV.

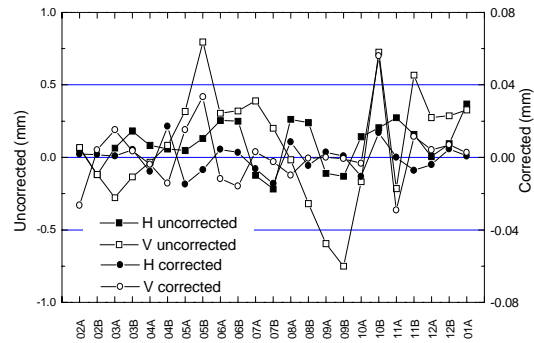


Figure 4: Orbit deviations with respect to the standard orbit. The *uncorrected* curves refer to the orbits obtained right after ramping to full energy.

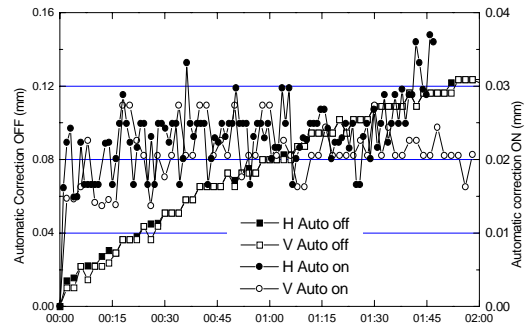


Figure 5: Variation of orbit envelopes as a function of time with the automatic correction system on and off.

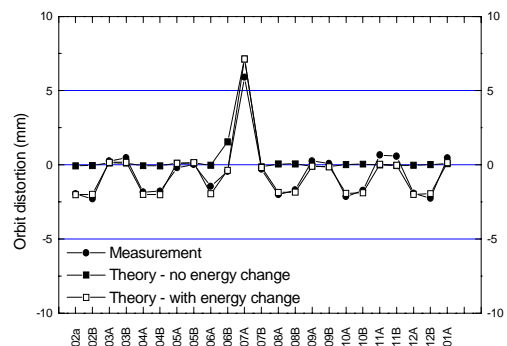


Figure 6: Measured and calculated horizontal localized orbit bumps. The calculations are done either with the correction matrix (Eq. 1) or with the inclusion of an energy change term.